THE JOURNAL OF PHYSICAL CHEMISTRY C
A JOURNAL OF THE AMERICAN CHEMICAL SOCIETY

pubs.acs.org/JPCC

Article

Mechanistic Insights into the Photocatalytic Hydrogen Production of Y5 and Y6 Nanoparticles

Andjela Brnovic, Leif Hammarström,* and Haining Tian*

Cite This: J. Phys. Chem. C 2023, 127, 12631−12639

Read Online

ACCESS | Metrics & More | Article Recommendations | Supporting Information

ABSTRACT: Utilization of solar energy in organic semiconductors relies on complicated photophysical processes due to the strong electron−hole interactions. To gain a better understanding of these processes and their effect on the photocatalytic performance of non-fullerene acceptors (NFAs) within nanoparticles (NPs), we compared the excited-state dynamics and photocatalytic hydrogen production activity of two NFA-based NPs, Y5 and Y6. Our results show that under LED light irradiation, Y5 NPs exhibit 14 times better hydrogen production activity than Y6 NPs. The hydrogen production activity was also evaluated under Xenon light irradiation (AM1.5G, 100 mW·cm^{-2}) for Y5 NPs, yielding 410 mmol/g after 24 h. Time-resolved spectroscopy experiments revealed a longer triplet lifetime for Y5 compared to Y6 NPs, and the lifetime was reduced upon addition of the electron donor ascorbate. This suggests the involvement of the triplet state in reductive quenching and better hydrogen evolution reaction performance for Y5 NPs. The good agreement between fluorescence and triplet lifetimes observed for Y5 NPs was attributed to reverse intersystem crossing, which repopulates the excited singlet state through thermally activated delayed fluorescence (TADF). The absence of TADF in Y6 NPs could limit its efficiency for hydrogen evolution reaction, in addition to the intrinsically shorter triplet lifetime and reduction potential difference, making it an important factor to consider in Y series-based NPs.

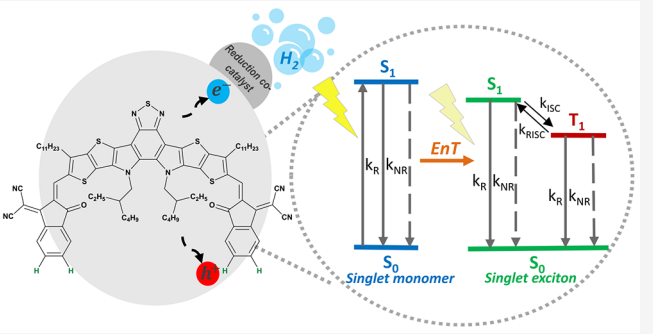

INTRODUCTION

Photocatalytic artificial photosynthesis has drawn great attention since it combines light-harvesting material properties with fuel production involving several photochemical steps: light absorption, charge separation, charge transport, charge transfer, surface reactions, transport of ions, reactants, and products. However, many challenges are still remaining to be addressed: fast charge recombination, low conversion efficiency, low selectivity of products, and poor stability.[1,2]

Organic semiconductors of earth-abundant elements have found their place in the photocatalytic field due to the tunable bandgaps, high extinction coefficients, and low cost.[3,4] Charge separation at the solid−liquid interface is one of the crucial photochemical steps but remains, however, a major bottleneck for their successful application. Due to the high exciton binding energy, spontaneous charge separation of electron−hole pairs at the interface is not efficient, making it challenging to drive surface catalytic reactions.[5−9] In light of this, research has been directed toward making hydrophobic polymers into hydrophilic nanoparticles (NPs).[10−13] Dispersing hydrophilic NPs into a medium with high dielectric constant such as water promotes dissociation of excitons at the NP−water interface. Also, confining polymers to nanosized particles decreases the distance required for exciton diffusion and at the same time increases the surface catalytic area, which improves overall photocatalytic performance.[10,11,14] Inspired by organic photovoltaics (OPVs), creating heterojunction donor−acceptor blend NPs has been implemented and reported in the literature as an efficient approach to promoting charge separation at the interface by using fullerene and non-fullerene acceptors (NFAs) to build up these heterojunctions.[15−22] Unlike fullerene acceptors, NFAs are more tunable, are more easily synthesized, and most importantly show increased absorption in the visible−NIR region, which is usually complementary to the absorption of the donor.[23,24] Moreover, NPs based on NFAs such as EH-IDTBR,[16] ITIC,[18] and Y6[25] and stabilized with surfactants that are not photo- or redox active have shown moderate photocatalytic hydrogen production activities. Dolan et al. tested Y6 NPs for photocatalytic hydrogen production and highlighted the impact of surfactants for their application.[26] In addition, molecular engineering of small-molecule photocatalysts showed significantly improved

Received: April 4, 2023
Revised: May 27, 2023
Published: June 22, 2023

photocatalytic hydrogen production, suggesting satisfactory charge separation in small-molecule NPs.[27−29] However, understanding the photophysical properties, particularly excitonic and charge separation processes in small-molecule NPs, is necessary for new molecular photocatalyst design. Excitonic effects and important excitonic processes set limitations to the overall photocatalytic quantum yield. Therefore, considering excitonic processes in NFAs is a promising approach toward their better design.

In this work, NPs of two well-known small organic NFAs, Y5 and Y6, were prepared to study and compare their excited-state dynamics. We highlighted their intrinsic differences and their effect on photocatalytic hydrogen production where Y5 NPs were shown to give better photocatalytic hydrogen production activity than Y6 NPs. By using steady-state and time-resolved spectroscopy, we gained more insight into the photocatalytic mechanism. A significantly longer photoluminescence lifetime of Y5 NPs was found compared to Y6 NPs assigned to thermally activated delayed fluorescence (TADF). Longer-lived species were observed for Y5 NPs and assigned to the Y5 triplet excited state, having an important role in a reductive quenching mechanism. Global analysis showed the existence of an intrinsically shorter-lived triplet for Y6 compared to Y5 NPs. In addition, no TADF was observed in Y6 NPs. These factors may explain the significantly different hydrogen evolution reaction performance between Y5 and Y6 NPs.

EXPERIMENTAL METHODS

Chemicals. NFAs: (2,2′-((2Z,2′Z)-((12,13-bis(2-ethylhexyl)-3,9-diundecyl-12,13-dihydro[1,2,5]thiadiazolo[3,4*e*]thieno-[2,″3:″4′,5′] thieno[2′,3′:4,5]pyrrolo[3,2-g] thieno[2′,3′:4,5]-thieno[3,2-*b*]indole-2,10-diyl)bis(methanylylidene))bis(3-oxo-2,3-dihydro1*H*-indene-2,1-diylidene))dimalononitrile) (**Y5**) and 2,2′-((2Z,2′Z)-((12,13-bis(2-ethylhexyl)-3,9-diundecyl-12,13-dihydro-[1,2,5]thiadiazolo[3,4-*e*]thieno[2″,3:″4′,5′]-thieno[2′,3′:4,5]pyrrolo[3,2-*g*]thieno[2′,3′:4,5]thieno[3,2-*b*]-indole-2,10-diyl)bis(methanylylidene))bis(5,6-difluoro-3-oxo-2,3-dihydro-1*H*-indene-2,1-diylidene))dimalononitrile (**Y6**) were purchased from Brilliant Matters and Sigma-Aldrich, respectively. Polystyrene grafted with ethylene oxide and carboxyl groups (PS−PEG−COOH, backbone chain M_w 8500, graft chain M_w 4600, total chain M_w 36,500) was purchased from Polymer Source Inc., Canada. Other reagents were purchased from Sigma-Aldrich and used as received. All experiments and measurements were carried out at room temperature.

Small Organic Molecule NPs Preparation. Y5 and Y6 NPs were prepared in the same manner according to the previously reported nanoprecipitation method procedures.[10,18] In more details, the first step involved preparing tetrahydrofuran (THF) solutions of respective small organic molecules and PS−PEG−COOH with 0.1 mg mL^{-1} concentrations and their mixing by keeping the ratio of molecule:PS−PEG−COOH 1:1.6 wt/wt. Subsequently, 4.8 mL of molecule:PS−PEG−COOH solution was rapidly dispersed into a 24 mL bulk aqueous phase (deionized water) and sonicated for 5 min. Finally, organic solvent was removed by keeping the samples in the dark at the room temperature overnight.

Photocatalytic Hydrogen Generation. A generated hydrogen amount was quantified by an HPR-20 benchtop gas analysis system (Hiden Analytical) using argon (Ar) as carrier gas. The experiments were carried out in gastight vials (9 mL volume). Aqueous potassium hexachloroplatinate solution (10 μL) was added into previously diluted 52 μg/mL molecular NP solutions (1.5 mL) and degassed with Ar for 15 min. Afterward, 0.5 mL of degassed 0.8 M L-ascorbic acid aqueous solution with pH = 4.2 (total concentration of L-ascorbic acid in the solution was 0.2 M) was added into the solutions. Ascorbic acid solution's pH was adjusted with 2 M KOH to obtain monodeprotonated ascorbic acid, ascorbate (ascorbic acid's first pK_a value is 4.17). The resulting solution was additionally degassed with Ar for 30 min to remove oxygen. Solutions were irradiated with an LED PAR38 lamp (17 W, 5000 K, Zenaro Lighting GmbH, $\lambda > 420$ nm) and a Xe lamp (300 W, AULTT CEL-HXF300/CEL-HXUV300) supplemented with an AM 1.5G filter. The light intensities of the irradiated area of the samples were measured with Thorlabs' optical power and an energy meter console (PM100D, Dachau, Germany). The light intensities of the LED lamp and Xenon lamp correspond to 50 and 100 mW cm^{-2}, respectively. Additionally, the setup was equipped with a fan to dissipate heat and maintain a lower temperature in the reaction environment.

External Quantum Efficiency. External quantum efficiency (EQE) was determined under the conditions used for photocatalytic hydrogen generation experiments in a 3.5 mL airtight quartz cuvette (path length 1 cm). The solution was illuminated by a 300 W Xe lamp (AULTT CEL-HXF300/CEL-HXUV300) as a light source equipped with an AM1.5 filter and different band pass filters (CEAULIGHT, 550 and 650) and LED array sources (Thorlabs' LIU780A and LIU780A, 750, 780, and 850) to select particular wavelengths. The hydrogen was measured by an HPR20 benchtop gas analysis system (Hiden Analytical) using Ar as carrier gas. The number of incident photons, N, was obtained by dividing the total energy (E_{total}) with the energy of one photon (E_{photon}):

$$N = \frac{E_{total}}{E_{photon}} = \frac{IS\lambda t}{hc}$$

where I is the irradiation density, S is the irradiation area, t is the irradiation time, h is Planck's constant, and c is the speed of light. EQE is defined as

$$\text{EQE}\ (\%) = \frac{2 \times \text{number of generated } H_2 \text{ molecules}}{\text{number of incident photons } (N)} \times 100$$

$$= \frac{2n_{H_2}N_A hc}{IS\lambda t} \times 100$$

where n_{H_2} represents the amount of hydrogen generated during the irradiation time and N_A is Avogadro's number.

Dynamic Light Scattering (DLS) Measurements. Hydrodynamic diameters were determined by utilizing a Zetasizer Nano S from Malvern Instruments Nordic AB.

Steady-State Spectroscopy. Absorption measurements were carried out on a PerkinElmer Lambda 750 UV−vis spectrophotometer. Steady-state emission measurements were recorded on a Fluorolog 3-222 emission spectrophotometer (Horiba Jobin-Yvon) together with the FluorEssence software using a right-angle detector geometry (90° angle), and corrections made for fluctuations in the light source and the detector response.

Time-Correlated Single Photon Counting (TCSPC). The fluorescence lifetime decays in the nanosecond range were measured on a Spectrofluorometer FS5 system from

https://doi.org/10.1021/acs.jpcc.3c02247
J. Phys. Chem. C 2023, 127, 12631−12639

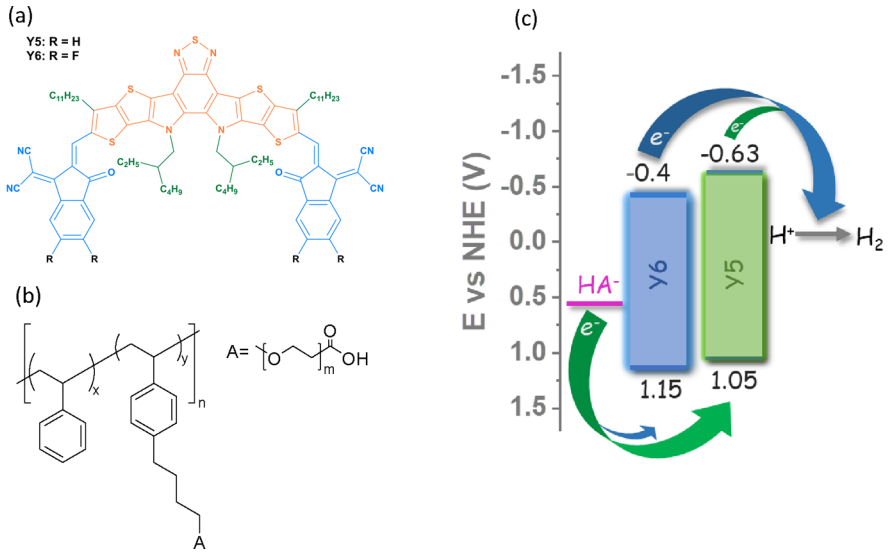

Figure 1. (a) Chemical structures of Y5 and Y6 with highlighted conjugated central backbone (orange), side chains (green), and terminal groups (blue). (b) Chemical structure of PS−PEG−COOH stabilizing surfactant. (c) Energy level scheme showing reduction potentials for Y5, Y6, ascorbate (pink), and proton reduction (gray) at pH = 4.2.

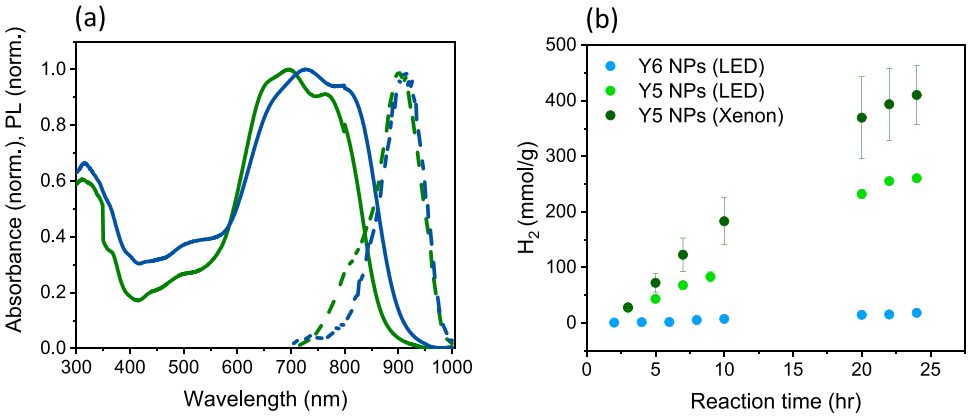

Figure 2. (a) Absorption (solid) and photoluminescence (PL) spectra (dashed) of Y5 NPs (green) and Y6 NPs (blue). (b) Hydrogen evolution versus time for Y5 and Y6 NPs under LED and Xenon light irradiation.

Edinburgh Instruments. The system was equipped with picosecond pulsed light emitting diode EPLED-470 with an excitation wavelength at 470 nm. The data were acquired in the 50 ns measurement range with the peak pre-set at 10^4 counts in 1024 channels. The scatter light profile (prompt signal) was recorded in a quartz cuvette (path length 1 cm) using diluted LUDOX solution in HPLC water at 470 nm emission wavelength. Molecule NP solutions were measured at the 870 nm emission wavelength. The obtained data was fitted using the DecayFit software.

Transient Absorption (TA) Measurements. All measurements were performed in water or THF at an ambient temperature. TA experiments were carried out using a Ti:sapphire-based amplifier with an integrated oscillator and pump lasers (Coherent Libra). The laser fundamental (800 nm, 3 kHz) was split into a pump and probe by a beam splitter, which were directed toward the UV−vis−NIR TA spectrometer (TAS, Newport Corp.). Pump wavelengths were obtained through optical parametric amplifiers (TOPAS NirUVis, Light Conversion). Prior to the sample cell, the pump was passed through a depolarizer and attenuated using a neutral density filter. Briefly, the probe supercontinuum was generated from a calcium fluoride or sapphire crystal (UV−vis) or YAG crystal (NIR) and its path was controlled by an optical delay ($t_{window} \leq 8$ ns), allowing the transient spectra at varying pump−probe delay times to be recorded on a silicon diode array (Newport custom-made). The instrument response function (IRF) was typically 130−150 fs, depending on the pump and probe wavelengths used. Depending on the probe region, cutoff filters were used. The samples were placed in quartz cuvettes (1 mm path length) and adjusted to the absorbance of ∼0.1−0.6 at the excitation wavelength. The measurements were performed with pump powers ranging from 10 to 350 μW (∼3.3−115 nJ/pulse) focused on the sample in a ca. 0.1 mm^2 spot.

All TA data sets were analyzed using Surface Xplorer for background extraction and time-zero correction and for fitting the chirp to a third-order polynomial function. Initially, the individual scans were analyzed carefully for inconsistencies, showing no indication of photodamage. Global analysis was performed by least-squares fitting using the R package TIMP and its GUI Glotaran. A sum of exponentials with wavelength-dependent amplitudes were fitted to the transient data using a parallel scheme, yielding decay-associated spectra (DAS).

https://doi.org/10.1021/acs.jpcc.3c02247
J. Phys. Chem. C 2023, 127, 12631−12639

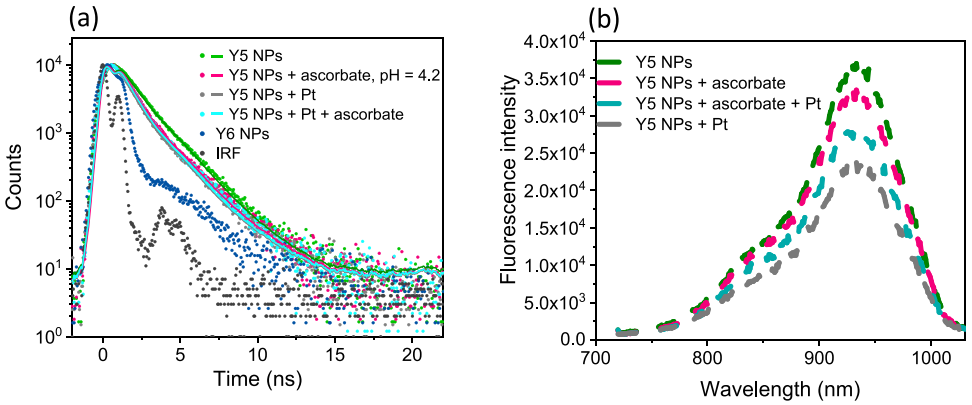

Figure 3. (a) Fluorescence decay kinetics of Y5 NPs convoluted with IRF and an exponential function with 1.4 ns lifetime (green), Y5 NPs and in situ photo-deposited Pt NPs (gray), Y5 NPs and sacrificial electron donor (ascorbate) (pink), Y5 NPs with in situ photo-deposited Pt NPs and added ascorbate (neon blue) and their corresponding fits (black), and Y6 NP fluorescence decay (blue). (b) Quenching of Y5 NP fluorescence emission intensity (green) by in situ Pt photo-deposition (gray), after adding a sacrificial electron donor (ascorbate) (pink), and after in situ photo-depositing Pt NPs and adding ascorbate (neon blue).

RESULTS AND DISCUSSION

Chemical structures of Y5, Y6, and PS−PEG−COOH are presented in Figure 1a,b. Unlike Y5, Y6 has fluorinated electron-deficient terminal end groups. A schematic representation of energy levels and corresponding standard potentials for reduction and oxidation were obtained from the literature according to the cyclic voltammetry in acetonitrile[30,31] (Figure 1c) as the average of the anodic and cathodic peak potentials. The scheme assumes that the potential for the excited-state reduction (Y^*/Y^-) is equal to that for the ground-state oxidation (Y^+/Y), i.e., the excitation energy $E_{00} = E^0_{(Y+/Y)} - E^0_{(Y/Y-)}$, which is typical for many organic dyes and semiconductor materials. It is shown that both molecules are thermodynamically able to reduce protons into molecular hydrogen and to be quenched by ascorbate as a sacrificial electron donor at pH = 4.2. Fluorinated electron-deficient terminal end groups of Y6 are responsible for shifting the energy levels and consequently narrowing the optical band gap.[32,33]

Y5 and Y6 NPs were prepared by the nanoprecipitation method according to the procedure described in the Experimental Methods. Absorption and photoluminescence (PL) spectra of Y5 and Y6 NPs are shown in Figure 2a and Figure S5. The absorption spectra of NPs in aqueous solutions are broad and red-shifted compared to those of the molecules dissolved in THF (Figure S1a,b). These bathochromic shifts were also observed in Y5 and Y6 films due to $\pi-\pi$ stacking.[34,35] Therefore, the spectra indicate a large degree of molecular $\pi-\pi$ stacking in Y5 and Y6 NPs as well, which extends the absorption of the light to the NIR region.

NPs were tested and compared for photocatalytic hydrogen evolution reaction (HER) (Figure 2b, Figure S2). Y5 NPs showed much higher HER activity than Y6 NPs, with an average amount of hydrogen after 24 h of 260 and 18 mmol/g for Y5 and Y6 NPs, respectively, under LED light irradiation (50 mW·cm^{-2}, 420−750 nm). The absorption of Y5 NPs is broadened up to 950 nm; thus, wavelengths above 750 nm are beyond the LED irradiation wavelength range. Furthermore, the HER for Y5 NPs was evaluated with a Xenon lamp (100 mW·cm^{-2}, AM1.5G) to encompass wavelengths in the NIR as well. Y5 NPs under Xenon lamp irradiation showed improved HER activity compared to the LED lamp, with an average amount of hydrogen of 410 mmol/g after 24 h. The maximum hydrogen generation rate is determined to be 22 mmol h^{-1} g^{-1}, which is comparable to the performance of most of polymer NP photocatalysts.[36]

The photocatalytic activity is in good agreement with EQE experiments where Y5 NPs exhibited modest EQEs of 0.37 and 0.13% at 750 and 850 nm, respectively (Figure S3). A maximum EQE value was obtained at 650 nm reaching 1%. Y5 NPs have a significantly higher EQE and hydrogen generation rate compared to the most recent report on TEBS-stabilized Y6 NPs with EQE of 0.054% at 780 nm and HER of 4.2 mmol/g h under Xenon lamp irradiation.[26] A decrease in EQEs toward NIR is consistent with reports for similar molecules used for photocatalytic hydrogen production.[25,27] This could be due to greater light penetration into the NP center and inefficient exciton diffusion to the water−NP interface in the large packing domains.

Although Y5 and Y6 have similar chemical structures and the same procedure was used for NP preparation, Y5 and Y6 NPs show a significant difference in HER activity. One contributing factor could be the lower driving force for proton reduction for Y6 NPs due to the 230 mV difference in reduction potentials (Figure 1b). Moreover, DLS measurements have also shown a larger hydrodynamic diameter of Y6 NPs compared to Y5 NPs, 100 and 60 nm for Y6 and Y5 NPs, respectively (Figure S4). A smaller hydrodynamic size of Y5 NPs could correspond to a larger surface catalytic area and a shorter exciton diffusion path, which influence better photocatalytic performance. Finally, differences in exciton and charge separation dynamics between the NPs may be important, which prompted a photophysical study.

Measurement of the fluorescence lifetime by TCSPC of Y5 and Y6 NPs (Figure 3a) was used to get more insights into the population and lifetime of photogenerated excitons. The fluorescence decay kinetics of Y5 NPs showed a lifetime of 1.4 ns, which is longer than what is reported for Y5 molecules in chloroform (450 ps).[37] Unlike Y5 NPs, the measured fluorescence decay of Y6 NPs was limited by the time resolution of TCSPC, implying a lifetime <240 ps. The IRF decay profile is shown in Figure 3a. The substantially longer fluorescence lifetime of Y5 NPs could allow more excitons to reach the interface and dissociate into free charges and thus be utilized in photocatalytic reaction.

https://doi.org/10.1021/acs.jpcc.3c02247
J. Phys. Chem. C 2023, 127, 12631−12639

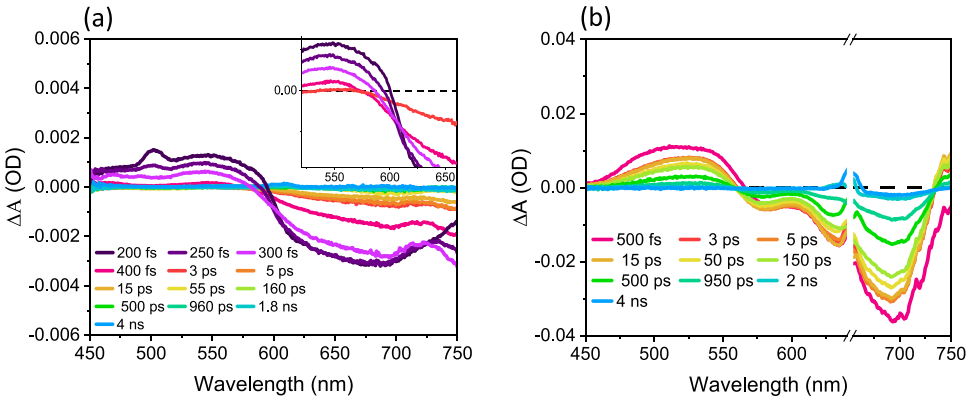

Figure 4. TA spectra in the visible region at different delay times for (a) Y5 NPs (16.5 nJ/pulse) with an inset showing the blue shift of isosbestic point and (b) Y5 dissolved in THF (115 nJ/pulse).

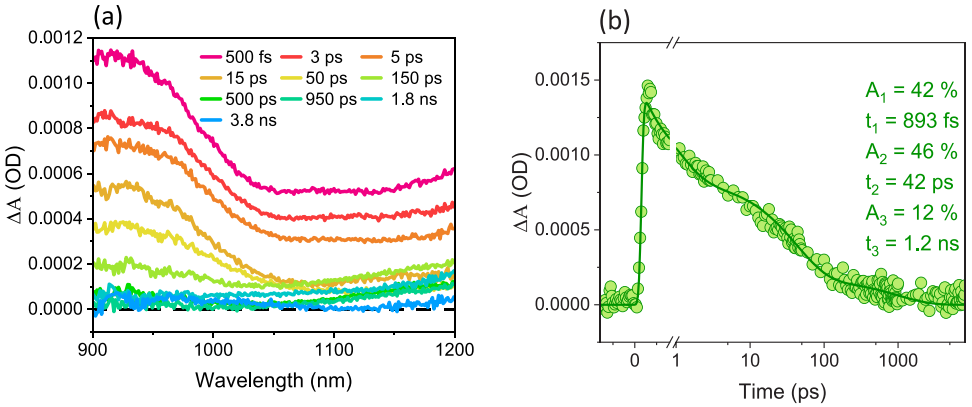

Figure 5. (a) TA spectra and (a) kinetics measured at 900 of Y5 NPs and 1200 nm after 650 nm excitation (16.5 nJ/pulse).

In order to understand the mechanism behind the photocatalytic performance of Y5 NPs, the effect of in situ photo-depositing Pt NPs and adding a sacrificial electron donor (ascorbate) on the lifetime of photogenerated excitons under similar conditions for HER experiments was investigated. Apart from comparing decay kinetics, the same absorbance at the excitation wavelength enabled us to compare number of counts per second acquired for different samples. Steady-state fluorescence quenching experiments were also performed under the same conditions. Reductive quenching by ascorbate decreased the PL lifetime (Figure 3a) and intensity (Figure 3b) by only 9%. Photo-deposition of Pt NPs decreased the PL lifetime to 950 ps and quenched almost 37% of the PL intensity, indicating potential electron/energy transfer to the Pt. However, photo-deposition of Pt NPs in the presence of ascorbate resulted in a PL lifetime of 1.1 ns (Figure 3a) as well as a 25% decrease in intensity (Figure 3b). The lower degree of quenching by Pt in the presence of ascorbate could indicate an interaction between the surface of NPs and ascorbate that can detach Pt NPs as they are not covalently bound but rather in situ photo-deposited on the surface of NPs.

To further investigate the excited-state decay processes involved in the photocatalytic mechanism of molecules in NPs, femtosecond TA measurements were performed in the visible (Figure 4a,b, Figures S6–S8) and NIR regions (Figures 5a,b and 6c, Figures S9–S14) after 650 nm excitation. The initial signal of Y5 NPs (Figure 4a) in the visible resembles that of Y5 in THF (Figure 4b), with excited-state absorption (ESA) bands at <600 nm and a negative signal maximizing around 680 nm; the latter is assigned to ground-state bleach (GSB), whereas stimulated emission was not apparent in the data for either Y5 NPs or Y5 in THF. Within 1 ps, the ESA decays almost completely, while a GSB signal above 720 nm grows in at the same time as the GSB at <700 nm recovers, partially causing the shift in the isosbestic point (inset, Figure 4a). The TA spectrum at >1 ps is assigned to delocalized excitons due to dye−dye interaction in the NPs. Thus, we assign the sub-ps process to excitation energy transfer from monomeric-like dye states to more delocalized exciton states. The recovery kinetics of the GSB band at 706 nm could be fitted with a sum of three exponents (Figure S6a), dominated by a time component of with τ_1 < 1 ps (66% amplitude), followed by two slower components with τ_2 = 20 ps (28%) and τ_3 = 1.1 ns (8%). In contrast, the dye in THF shows a single-exponential decay with lifetime of 560 ps at 625 nm (Figure S6b), in good agreement with literature data for the same molecule in chloroform.[37] Thus, most of the excited states are more short-lived in the NPs. The results for NPs were essentially invariant with a pump power up to 50 μW (Figure S7a). At higher pump powers, from 0.1 to 0.35 μW, the τ_1 < 1 ps component increased in relative amplitude and became shorter in lifetime (Figure S7b). This is assigned to biexcitonic decay processes, which are common deactivation pathways at higher pump powers.[38] Y6 NPs showed similar TA spectral features and dynamics to Y5 NPs in the visible region (Figure S8a,b).

Experiments probing the NIR region of the dyes in THF showed a strong ESA at 900 nm that decreased with increasing wavelength and a weaker band increasing from 1000 to 1200

https://doi.org/10.1021/acs.jpcc.3c02247
J. Phys. Chem. C 2023, 127, 12631−12639

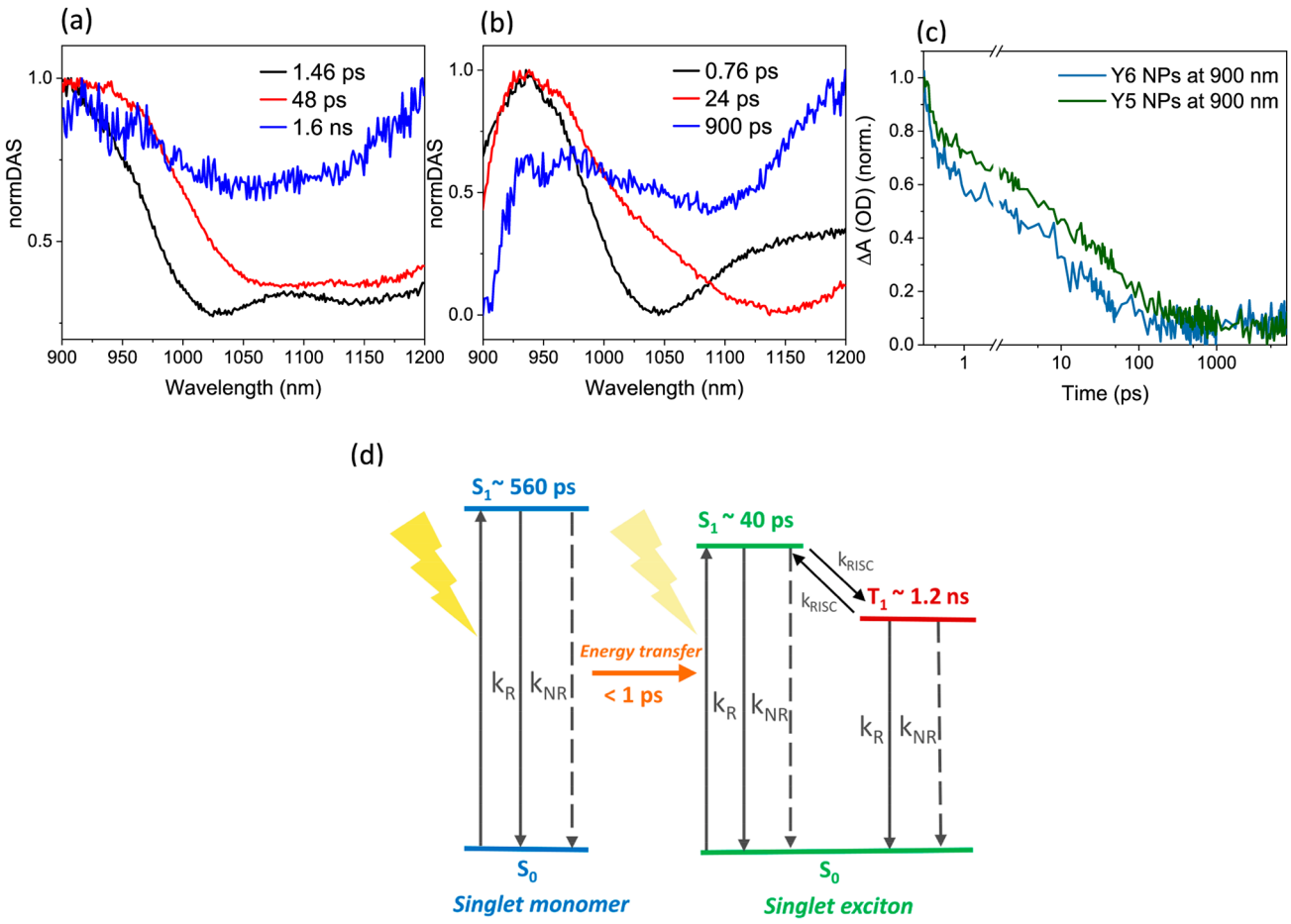

Figure 6. Normalized DAS (a, b) obtained from global analysis of the data presented in Figure 5a and Figure S10a for Y5 and Y6 NPs, respectively. (c) Normalized TA kinetics of Y5 and Y6 NPs measured with 650 nm excitation at 900 nm (16.5 nJ/pulse). (d) Schematic representation (Jablonski diagram) showing the excitonic processes in photoexcited Y5 NPs.

nm (Figures S9 and S10b). Singlet excited-state lifetimes in THF were also determined in the NIR region by monitoring kinetics at 900 nm, 500 and 730 ps for Y5 and Y6 (Figure S11a and b), respectively, in good agreement with the data from the visible region. For the NPs, the ESA was red-shifted with a maximum around 930 nm and much stronger absorption at the higher wavelengths. (Figure 5a; data for Y6 NPs in Figure S10a). A tri-exponential fit to the kinetic trace at 900 nm for Y5 NPs in Figure 5b gave similar results as for the GSB recovery at 706 nm: τ_1 < 1 ps (42%), τ_2 = 42 ps (46%), and τ_3 = 1.2 ns (10%).

The TA spectral evolution with time in the NIR region was successfully fitted globally using a three-exponential model with associated time components of τ_1 = 1.5 ps, τ_2 = 48 ps, and τ_3 = 1.6 ns for Y5 NPs (Figure 6a). The DAS represent gain and loss in the absorption of these three lifetime components. The first and second DAS (τ_1 and τ_2, respectively) for both dyes within NPs have similar shapes, showing a loss of the positive features at all wavelengths, although the relative loss is more significant at <1000 nm. The third DAS (τ_3) is instead dominated by decay of the positive signal at longer wavelengths (>1000 nm) which probably extends above 1200 nm (Figure 6a,b). A recent literature report on Y6 thin films highlighted the existence of a weak long-lived positive signal at wavelengths from ca. 1100 nm, increasing with increasing wavelength.[38] This was attributed to the triplet excitons formed through intersystem crossing (ISC) at low excitation fluences, favored due to the small energy gap between excited singlet and triplet states (< 0.3 eV). The spectral shape of the 900 ps component in Figure 6b is consistent with formation of the triplet excited state, with remaining positive contributions around 900−1000 nm from the singlet state. Overall lifetimes are shorter for Y6 NPs (τ_2 = 24 ps and τ_3 = 900 ps) compared to Y5 NPs (Figure 6a,b) and by inspecting normalized kinetic traces at 900 nm for Y5 and Y6 NPs (Figure 6c). Selected kinetic traces from the global analysis data are shown in Figure S13a,b.

The three kinetic components can be understood as follows, as presented in the Jablonski diagram in Figure 6d. Most of the excitons corresponding to τ_1 decayed within <1 ps, which we assigned to the energy transfer from monomeric dyes to excitonic states, because of the similarity of the initial TA spectra to that in THF (Figure 4b). Excitons with an ∼40 ps lifetime for Y5 NPs (24 ps for Y6 NPs) most likely represent the intrinsic singlet exciton lifetime being substantially shorter than what is observed for the same molecule in organic solvent (τ ∼ 0.5 ns, Figure S11a). This can be attributed, at least partly, to the ISC process resulting in triplet excitons with a 1.2 ns lifetime corresponding to τ_3 shown with ca. 10% amplitude of the GSB recovery.

In the recent report cited above, the authors reflected on the apparent discrepancy between the fluorescence lifetime from

https://doi.org/10.1021/acs.jpcc.3c02247
J. Phys. Chem. C 2023, 127, 12631−12639

TCSPC and femtosecond TA for singlet exciton lifetime in Y6 films.[38] Triplet−triplet exciton annihilation (TTA) was proposed as the possible pathway that repopulates the singlet excited state and results in delayed fluorescence (DF), reflecting triplet excited-state lifetime. Interestingly, the 1.4 ns fluorescence lifetime obtained from the present TCSPC experiment (Figure 3a) is similar to the longest, τ_3 lifetime obtained from TA and global analysis for Y5 NPs in the low linear power regime unlike for Y6 NPs where the fluorescence lifetime was within IRF. Thus, we propose reverse intersystem crossing (RISC) at ambient temperatures characteristic for TADF for Y5 NPs, probably due to a smaller singlet−triplet energy gap for Y5 than for Y6 NPs. To verify the origin of DF, we examined the excitation intensity dependence of the fluorescence intensity[39] (Figure 7). As a linear dependence was

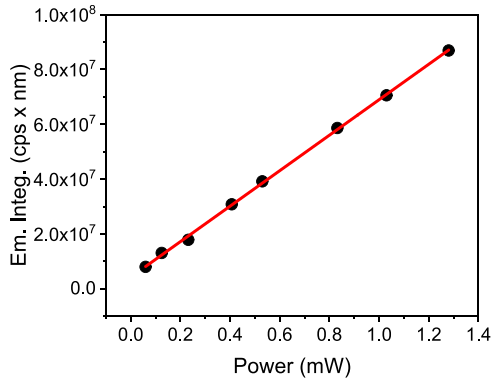

Figure 7. Variation of the steady-state fluorescence intensity with excitation intensity.

found, we concluded that the excited singlet state of Y5 NPs is mainly repopulated through RISC and, therefore, TADF. We could thus exclude TTA, which would have shown a quadratic intensity dependence at these moderate excitation intensities and considering that TA experiments were performed in the linear power regime.[39−41] Although TADF is an intramolecular process and could in principle be observed in the molecules in organic solvents as well, we assume that the different environment and excitonic interactions in the NPs significantly alter the singlet−triplet energy gap.

High exciton binding energies reported for NFAs, although lower than for fullerenes, still prevent higher yield of charge separation in photocatalytic conditions.[42] To investigate potential intercomponent charge separation reactions and understand the role of the excited triplet state and TADF observed for Y5 NPs, TA experiments were performed in the NIR region under similar conditions as those used for photocatalytic HER. Fits to the kinetic trace at 900 nm after addition of 0.2 M ascorbate at pH = 4.2 showed a decrease in all time constants, and the triplet lifetime decreased from 1.2 ns to 250 ps (Figure 8a, Figure S14a). This highlights the importance of triplet-state involvement in reductive quenching in Y5 NPs. Overall lifetime quenching was observed with photo-deposited Pt NPs as well, with and without ascorbate, in good agreement with TCSPC results (Figure 8b,c, Figure S14b,c). A comprehensive summary of all fitted values obtained from the femtosecond TA experiments in the NIR and visible regions can be found in Table S1.

The triplet lifetime of Y6 NPs is only somewhat shorter than for Y5 NPs (0.9 and 1.6 ns for Y6 and Y5 NPs, respectively, according to the global analysis results) and can hardly explain the large difference in photocatalytic activity. The absence of observable TADF for Y6 NPs, i.e., fluorescence with a lifetime corresponding to that of the triplet state, suggests a larger singlet−triplet energy gap. It is possible that charge separation occurs mainly via the singlet state and that the inefficient repopulation of the singlet is one reason for its low photocatalytic activity.

CONCLUSIONS

In conclusion, we have compared Y5 and Y6 NPs for photocatalytic hydrogen production and revealed a better HER activity of Y5 NPs (410 mmol/g after 24 h) comparable to most of polymer nano-photocatalysts.[36] The TA study of Y5 NPs showed the existence of longer-lived components corresponding to the excited triplet state and its involvement in reductive quenching by ascorbate at pH = 4.2 supported by TCSPC and TA experiments as well as global analysis. The existence of TADF as a mechanism that repopulates the excited singlet state through RISC in Y5 NPs was elucidated through the linear variation of the steady-state fluorescence intensity with excitation intensity. This opens the possibility to further investigate the role of TADF in photocatalytic reactions since the research so far is scarce in this area. Correlated with the triplet-state involvement in the reductive quenching mechanism, the much better photocatalytic performance of Y5 NPs may be explained by its longer-lived triplet state, the presence of TADF, and the more reducing potential. An

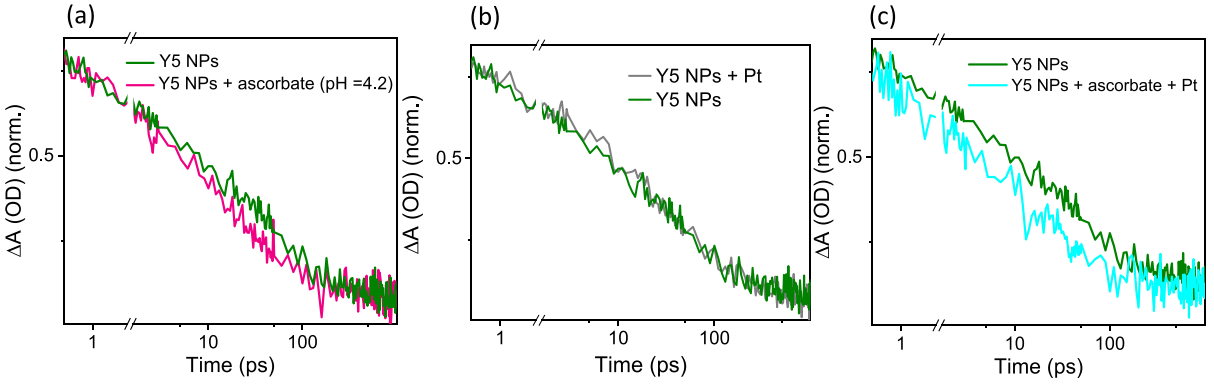

Figure 8. TA kinetics of Y5 NPs measured with 650 nm excitation with 0.2 M ascorbate at pH = 4.2 (a), with in situ photo-deposited Pt NPs (b), and with in situ photo-deposited Pt NPs and ascorbate at pH = 4.2 (c) (16.5 nJ/pulse).

https://doi.org/10.1021/acs.jpcc.3c02247
J. Phys. Chem. C 2023, 127, 12631−12639

additional factor may be the larger size of Y6 NPs, which may hamper efficient charge separation at the NP interface. The moderate EQEs in the NIR region and improved photocatalytic activity for HER of Y5 compared to Y6 NPs leave room for developing new NIR light-activated photocatalysts since, to date, only few have been reported to efficiently harvest NIR light.

■ ASSOCIATED CONTENT

Supporting Information

The Supporting Information is available free of charge at https://pubs.acs.org/doi/10.1021/acs.jpcc.3c02247.

Absorption and fluorescence spectra; photostability data before and after 24 h of irradiation under LED and Xenon lamp illumination; EQEs of Y5 NPS at different absorption wavelengths; DLS results; TA spectra and kinetic traces in water and THF including fluence dependence for Y5 NPs; selected kinetic traces from the global analysis; a table with an overview of the fitting results (PDF)

■ AUTHOR INFORMATION

Corresponding Authors

Leif Hammarström − *Department of Chemistry, Ångström Laboratory, Uppsala University, SE 751 20 Uppsala, Sweden;* orcid.org/0000-0002-9933-9084; Email: leif.hammarstrom@kemi.uu.se

Haining Tian − *Department of Chemistry, Ångström Laboratory, Uppsala University, SE 751 20 Uppsala, Sweden;* orcid.org/0000-0001-6897-2808; Email: haining.tian@kemi.uu.se

Author

Andjela Brnovic − *Department of Chemistry, Ångström Laboratory, Uppsala University, SE 751 20 Uppsala, Sweden;* orcid.org/0000-0001-5166-4163

Complete contact information is available at: https://pubs.acs.org/10.1021/acs.jpcc.3c02247

Notes

The authors declare no competing financial interest.

■ ACKNOWLEDGMENTS

We would like to thank the financial support from the Wallenberg Academy Fellow program in K&A Wallenberg Foundation. We are thankful to Nora Eliasson (UU) for her kind help with the femtosecond laser and discussion, Dr. Victor Gray (UU) for the discussion, and Nidhi Kaul (UU) and Dr. Hongwei Song (UU) for discussions and help with global analysis.

■ REFERENCES

(1) Kosco, J.; Moruzzi, F.; Willner, B.; McCulloch, I. Photocatalysts Based on Organic Semiconductors with Tunable Energy Levels for Solar Fuel Applications. *Adv. Energy Mater.* **2020**, *10*, No. 2001935.

(2) Yanagi, R.; Zhao, T.; Solanki, D.; Pan, Z.; Hu, S. Charge Separation in Photocatalysts: Mechanisms, Physical Parameters, and Design Principles. *ACS Energy Lett.* **2022**, *7*, 432−452.

(3) Martin, D. J.; Reardon, P. J. T.; Moniz, S. J. A.; Tang, J. Visible Light-Driven Pure Water Splitting by a Nature-Inspired Organic Semiconductor-Based System. *J. Am. Chem. Soc.* **2014**, *136*, 12568−12571.

(4) Weingarten, A. S.; Kazantsev, R. V.; Palmer, L. C.; Fairfield, D. J.; Koltonow, A. R.; Stupp, S. I. Supramolecular Packing Controls H_2 Photocatalysis in Chromophore Amphiphile Hydrogels. *J. Am. Chem. Soc.* **2015**, *137*, 15241−15246.

(5) Koch, S. W.; Kira, M.; Khitrova, G.; Gibbs, H. M. Semiconductor Excitons in New Light. *Nat. Mater.* **2006**, *5*, 523−531.

(6) Scholes, G. D.; Rumbles, G. Excitons in Nanoscale Systems. *Nat. Mater.* **2010**, *5*, 12−25.

(7) Zhu, L.; Yi, Y.; Wei, Z. Exciton Binding Energies of Nonfullerene Small Molecule Acceptors: Implication for Exciton Dissociation Driving Forces in Organic Solar Cells. *J. Phys. Chem. C* **2018**, *122*, 22309−22316.

(8) Wang, Y.; Vogel, A.; Sachs, M.; Sprick, R. S.; Wilbraham, L.; Moniz, S. J. A.; Godin, R.; Zwijnenburg, M. A.; Durrant, J. R.; Cooper, A. I.; et al. Current Understanding and Challenges of Solar-Driven Hydrogen Generation Using Polymeric Photocatalysts. *Nat. Energy* **2019**, *4*, 746−760.

(9) Gledhill, S. E.; Scott, B.; Gregg, B. A. Organic and Nano-Structured Composite Photovoltaics: An Overview. *J. Mater. Res.* **2005**, *20*, 3167−3179.

(10) Wang, L.; Fernández-Terán, R.; Zhang, L.; Fernandes, D. L. A.; Tian, L.; Chen, H.; Tian, H. Organic Polymer Dots as Photocatalysts for Visible Light-Driven Hydrogen Generation. *Angew. Chem., Int. Ed.* **2016**, *55*, 12306−12310.

(11) Pati, P. B.; Damas, G.; Tian, L.; Fernandes, D. L. A.; Zhang, L.; Pehlivan, I. B.; Edvinsson, T.; Araujo, C. M.; Tian, H. An Experimental and Theoretical Study of an Efficient Polymer Nano-Photocatalyst for Hydrogen Evolution. *Energy Environ. Sci.* **2017**, *10*, 1372−1376.

(12) Tseng, P. J.; Chang, C. L.; Chan, Y. H.; Ting, L. Y.; Chen, P. Y.; Liao, C. H.; Tsai, M. L.; Chou, H. H. Design and Synthesis of Cycloplatinated Polymer Dots as Photocatalysts for Visible-Light-Driven Hydrogen Evolution. *ACS Catal.* **2018**, *8*, 7766−7772.

(13) Hu, Z.; Wang, Z.; Zhang, X.; Tang, H.; Liu, X.; Huang, F.; Cao, Y. Conjugated Polymers with Oligoethylene Glycol Side Chains for Improved Photocatalytic Hydrogen Evolution. *iScience* **2019**, *13*, 33−42.

(14) Liu, A.; Tai, C. W.; Holá, K.; Tian, H. Hollow Polymer Dots: Nature-Mimicking Architecture for Efficient Photocatalytic Hydrogen Evolution Reaction. *J. Mater. Chem. A* **2019**, *7*, 4797−4803.

(15) Fortin, P.; Rajasekar, S.; Chowdhury, P.; Holdcroft, S. Hydrogen Evolution at Conjugated Polymer Nanoparticle Electrodes. *Can. J. Chem.* **2018**, *96*, 148−157.

(16) Kosco, J.; Bidwell, M.; Cha, H.; Martin, T.; Howells, C. T.; Sachs, M.; Anjum, D. H.; Gonzalez Lopez, S.; Zou, L.; Wadsworth, A.; et al. Enhanced Photocatalytic Hydrogen Evolution from Organic Semiconductor Heterojunction Nanoparticles. *Nat. Mater.* **2020**, *19*, 559−565.

(17) Yang, H.; Li, X.; Sprick, R. S.; Cooper, A. I. Conjugated Polymer Donor−Molecular Acceptor Nanohybrids for Photocatalytic Hydrogen Evolution. *Chem. Commun.* **2020**, *56*, 6790−6793.

(18) Liu, A.; Gedda, L.; Axelsson, M.; Pavliuk, M.; Edwards, K.; Hammarström, L.; Tian, H. Panchromatic Ternary Polymer Dots Involving Sub-Picosecond Energy and Charge Transfer for Efficient and Stable Photocatalytic Hydrogen Evolution. *J. Am. Chem. Soc.* **2021**, *143*, 72875−72885.

(19) Yang, Y.; Li, D.; Wang, P.; Zhang, X.; Zhang, H.; Du, B.; Guo, C.; Wang, T.; Liu, D. Polymer/Non-Fullerene Acceptor Bulk Heterojunction Nanoparticles for Efficient Photocatalytic Hydrogen Production from Water. *Polymer (Guildf).* **2022**, *244*, No. 124667.

(20) Zhao, H.; Dong, Y.; Sun, P.; Bai, Y.; Ru, C.; Wu, X.; Li, Z.; Han, X.; Wu, J.; Pan, X. Effect of D/A Ratio on Photocatalytic Hydrogen Evolution Performance of Conjugated Polymer Photocatalysts. *ACS Appl. Energy Mater.* **2022**, *5*, 4631−4640.

(21) Elsayed, M. H.; Abdellah, M.; Hung, Y. H.; Jayakumar, J.; Ting, L. Y.; Elewa, A. M.; Chang, C. L.; Lin, W. C.; Wang, K. L.; Abdel-Hafiez, M.; et al. Hydrophobic and Hydrophilic Conjugated Polymer Dots as Binary Photocatalysts for Enhanced Visible-Light-Driven

Hydrogen Evolution through Förster Resonance Energy Transfer. *ACS Appl. Mater. Interfaces* **2021**, *13*, 56554−56565.
(22) Zhang, Z.; Si, W.; Wu, B.; Wang, W.; Li, Y.; Ma, W.; Lin, Y. Two-Dimensional Polycyclic Photovoltaic Molecule with Low Trap Density for High-Performance Photocatalytic Hydrogen Evolution. *Angew. Chem., Int. Ed.* **2022**, *61*, 1−8.
(23) Lin, Y.; Wang, J.; Zhang, Z. G.; Bai, H.; Li, Y.; Zhu, D.; Zhan, X. An Electron Acceptor Challenging Fullerenes for Efficient Polymer Solar Cells. *Adv. Mater.* **2015**, *27*, 1170−1174.
(24) Feng, L.; Yuan, J.; Zhang, Z.; Peng, H.; Zhang, Z. G.; Xu, S.; Liu, Y.; Li, Y.; Zou, Y. Thieno[3,2-b]Pyrrolo-Fused Pentacyclic Benzotriazole-Based Acceptor for Efficient Organic Photovoltaics. *ACS Appl. Mater. Interfaces* **2017**, *9*, 31985−31992.
(25) Kosco, J.; Gonzalez-Carrero, S.; Howells, C. T.; Fei, T.; Dong, Y.; Sougrat, R.; Harrison, G. T.; Firdaus, Y.; Sheelamanthula, R.; Purushothaman, B.; et al. Generation of Long-Lived Charges in Organic Semiconductor Heterojunction Nanoparticles for Efficient Photocatalytic Hydrogen Evolution. *Nat. Energy* **2022**, *7*, 340−351.
(26) Dolan, A.; Perrelle, J. M.; Milsom, E. R.; Small, T. D.; Metha, G. F.; Pan, X.; Andersson, M. R.; Huang, D. M. Surfactant Effects on Hydrogen Evolution by Small Molecule Non-Fullerene Acceptor Nanoparticles. *ACS Appl. Nano Mater.* **2022**, *5*, 12154−12164.
(27) Zhu, Y.; Zhang, Z.; Si, W.; Sun, Q.; Cai, G.; Li, Y.; Jia, Y.; Lu, X.; Xu, W.; Zhang, S.; et al. Organic Photovoltaic Catalyst with Extended Exciton Diffusion for High-Performance Solar Hydrogen Evolution. *J. Am. Chem. Soc.* **2022**, *144*, 12747−12755.
(28) Yang, H.; Li, C.; Liu, T.; Fellowes, T.; Chong, S. Y.; Catalano, L.; Bahri, M.; Zhang, W.; Xu, Y.; Liu, L.; et al. Packing-Induced Selectivity Switching in Molecular Nanoparticle Photocatalysts for Hydrogen and Hydrogen Peroxide Production. *Nat. Nanotechnol.* **2023**, *18*, 307−315.
(29) Liang, Y.; Li, T.; Lee, Y.; Zhang, Z.; Li, Y.; Si, W.; Liu, Z.; Zhang, C.; Qiao, Y.; Bai, S.; et al. Organic Photovoltaic Catalyst with σ-π Anchor for High-Performance Solar Hydrogen Evolution. *Angew. Chem., Int. Ed.* **2023**, 62.
(30) Yuan, J.; Zhang, Y.; Zhou, L.; Zhang, C.; Lau, T. K.; Zhang, G.; Lu, X.; Yip, H. L.; So, S. K.; Beaupré, S.; et al. Fused Benzothiadiazole: A Building Block for n-Type Organic Acceptor to Achieve High-Performance Organic Solar Cells. *Adv. Mater.* **2019**, *31*, 1−8.
(31) Yuan, J.; Zhang, Y.; Zhou, L.; Zhang, G.; Yip, H. L.; Lau, T. K.; Lu, X.; Zhu, C.; Peng, H.; Johnson, P. A.; et al. Single-Junction Organic Solar Cell with over 15% Efficiency Using Fused-Ring Acceptor with Electron-Deficient Core. *Joule* **2019**, *3*, 1140−1151.
(32) Zhang, Q.; Kelly, M. A.; Bauer, N.; You, W. The Curious Case of Fluorination of Conjugated Polymers for Solar Cells. *Acc. Chem. Res.* **2017**, *50*, 2401−2409.
(33) Dai, S.; Zhao, F.; Zhang, Q.; Lau, T. K.; Li, T.; Liu, K.; Ling, Q.; Wang, C.; Lu, X.; You, W.; et al. Fused Nonacyclic Electron Acceptors for Efficient Polymer Solar Cells. *J. Am. Chem. Soc.* **2017**, *139*, 1336−1343.
(34) Lai, H.; He, F. Crystal Engineering in Organic Photovoltaic Acceptors: A 3D Network Approach. *Adv. Energy Mater.* **2020**, *10*, 1−16.
(35) Kupgan, G.; Chen, X. K.; Brédas, J. L. Molecular Packing of Non-Fullerene Acceptors for Organic Solar Cells: Distinctive Local Morphology in Y6 vs ITIC Derivatives. *Mater. Today Adv.* **2021**, *11*, No. 100154.
(36) Pavliuk, M. V.; Wrede, S.; Liu, A.; Brnovic, A.; Wang, S.; Axelsson, M.; Tian, H. Preparation, Characterization, Evaluation and Mechanistic Study of Organic Polymer Nano-Photocatalysts for Solar uel Production. *Chem. Soc. Rev.* **2022**, *51*, 6909−6935.
(37) Wen, G.; Hu, R.; Su, X.; Chen, Z.; Zhang, C.; Peng, J.; Zou, X.; He, X.; Dong, G.; Zhang, W. Excited-State Properties of Y-Series Small Molecule Semiconductors. *Dyes Pigm.* **2021**, *192*, No. 109431.
(38) Natsuda, S. I.; Sakamoto, Y.; Takeyama, T.; Shirouchi, R.; Saito, T.; Tamai, Y.; Ohkita, H. Singlet and Triplet Excited-State Dynamics of a Nonfullerene Electron Acceptor Y6. *J. Phys. Chem. C* **2021**, *125*, 20806−20813.
(39) Dias, F. B. Kinetics of Thermal-Assisted Delayed Fluorescence in Blue Organic Emitters with Large Singlet-Triplet Energy Gap. *Philos. Trans. R. Soc., A* **2015**, *373*, No. 20140447.
(40) Hertel, D.; Bässler, H.; Guentner, R.; Schert, U. Triplet-Triplet Annihilation in a Poly(Fluorene)-Derivative. *J. Chem. Phys.* **2001**, *115*, 10007−10013.
(41) Jankus, V.; Snedden, E. W.; Bright, D. W.; Whittle, V. L.; Williams, J. A. G.; Monkman, A. Energy Upconversion via Triplet Fusion in Super Yellow PPV Films Doped with Palladium Tetraphenyltetrabenzoporphyrin: A Comprehensive Investigation of Exciton Dynamics. *Adv. Funct. Mater.* **2013**, *23*, 384−393.
(42) Benatto, L.; Marchiori, C. F. N.; Moyses Araujo, C.; Koehler, M. Molecular Origin of Efficient Hole Transfer from Non-Fullerene Acceptors: Insights from First-Principles Calculations. *J. Mater. Chem. C* **2019**, *7*, 12180−12193.

https://doi.org/10.1021/acs.jpcc.3c02247
J. Phys. Chem. C 2023, 127, 12631−12639